
Understanding Batch Normalization

Johan Bjorck, Carla Gomes, Bart Selman, Kilian Q. Weinberger
Cornell University
{njb225,gomes,selman,kqw4}@cornell.edu

Abstract

Batch normalization (BN) is a technique to normalize activations in intermediate layers of deep neural networks. Its tendency to improve accuracy and speed up training have established BN as a favorite technique in deep learning. Yet, despite its enormous success, there remains little consensus on the exact reason and mechanism behind these improvements. In this paper we take a step towards a better understanding of BN, following an empirical approach. We conduct several experiments, and show that BN primarily enables training with larger learning rates, which is the cause for faster convergence and better generalization. For networks without BN we demonstrate how large gradient updates can result in diverging loss and activations growing uncontrollably with network depth, which limits possible learning rates. BN avoids this problem by constantly correcting activations to be zero-mean and of unit standard deviation, which enables larger gradient steps, yields faster convergence and may help bypass sharp local minima. We further show various ways in which gradients and activations of deep unnormalized networks are ill-behaved. We contrast our results against recent findings in random matrix theory, shedding new light on classical initialization schemes and their consequences.

1 Introduction

Normalizing the input data of neural networks to zero-mean and constant standard deviation has been known for decades [29] to be beneficial to neural network training. With the rise of deep networks, Batch Normalization (BN) naturally extends this idea across the intermediate layers within a deep network [23], although for speed reasons the normalization is performed across mini-batches and not the entire training set. Nowadays, there is little disagreement in the machine learning community that BN accelerates training, enables higher learning rates, and improves generalization accuracy [23] and BN has successfully proliferated throughout all areas of deep learning [2, 17, 21, 46]. However, despite its undeniable success, there is still little consensus on why the benefits of BN are so pronounced. In their original publication [23] Ioffe and Szegedy hypothesize that BN may alleviate “internal covariate shift” – the tendency of the distribution of activations to drift during training, thus affecting the inputs to subsequent layers. However, other explanations such as improved stability of concurrent updates [13] or conditioning [42] have also been proposed.

Inspired by recent empirical insights into deep learning [25, 36, 57], in this paper we aim to clarify these vague intuitions by placing them on solid experimental footing. We show that the activations and gradients in deep neural networks without BN tend to be heavy-tailed. In particular, during an early on-set of divergence, a small subset of activations (typically in deep layer) “explode”. The typical practice to avoid such divergence is to set the learning rate to be sufficiently small such that no steep gradient direction can lead to divergence. However, small learning rates yield little progress along flat directions of the optimization landscape and may be more prone to convergence to sharp local minima with possibly worse generalization performance [25].

BN avoids activation explosion by repeatedly correcting all activations to be zero-mean and of unit standard deviation. With this “safety precaution”, it is possible to train networks with large learning

rates, as activations cannot grow incontrollably since their means and variances are normalized. SGD with large learning rates yields faster convergence along the flat directions of the optimization landscape and is less likely to get stuck in sharp minima.

We investigate the interval of viable learning rates for networks with and without BN and conclude that BN is much more forgiving to very large learning rates. Experimentally, we demonstrate that the activations in deep networks without BN grow dramatically with depth if the learning rate is too large. Finally, we investigate the impact of random weight initialization on the gradients in the network and make connections with recent results from random matrix theory that suggest that traditional initialization schemes may not be well suited for networks with many layers — unless BN is used to increase the network’s robustness against ill-conditioned weights.

1.1 The Batch Normalization Algorithm

As in [23], we primarily consider BN for convolutional neural networks. Both the input and output of a BN layer are four dimensional tensors, which we refer to as $I_{b,c,x,y}$ and $O_{b,c,x,y}$, respectively. The dimensions corresponding to examples within a batch b , channel c , and two spatial dimensions x, y respectively. For input images the channels correspond to the RGB channels. BN applies the same normalization for all activations in a given channel,

$$O_{b,c,x,y} \leftarrow \gamma_c \frac{I_{b,c,x,y} - \mu_c}{\sqrt{\sigma_c^2 + \epsilon}} + \beta_c \quad \forall b, c, x, y. \tag{1}$$

Here, BN subtracts the mean activation $\mu_c = \frac{1}{|\mathcal{B}|} \sum_{b,x,y} I_{b,c,x,y}$ from all input activations in channel c , where \mathcal{B} contains all activations in channel c across all features b in the entire mini-batch and all spatial x, y locations. Subsequently, BN divides the centered activation by the standard deviation σ_c (plus ϵ for numerical stability) which is calculated analogously. During testing, running averages of the mean and variances are used. Normalization is followed by a channel-wise affine transformation parametrized through γ_c, β_c , which are learned during training.

1.2 Experimental Setup

To investigate batch normalization we will use an experimental setup similar to the original Resnet paper [17]: image classification on CIFAR10 [27] with a 110 layer Resnet. We use SGD with momentum and weight decay, employ standard data augmentation and image preprocessing techniques and decrease learning rate when learning plateaus, all as in [17] and with the same parameter values. The original network can be trained with initial learning rate 0.1 over 165 epochs, however which fails without BN. We always report the best results among initial learning rates from $\{0.1, 0.003, 0.001, 0.0003, 0.0001, 0.00003\}$ and use enough epochs such that learning plateaus. For further details, we refer to Appendix B in the online version [4].

2 Disentangling the benefits of BN

Without batch normalization, we have found that the initial learning rate of the Resnet model needs to be decreased to $\alpha = 0.0001$ for convergence and training takes roughly 2400 epochs. We refer to this architecture as an unnormalized network. As illustrated in Figure 1 this configuration does not attain the accuracy of its normalized counterpart. Thus, seemingly, batch normalization yields faster training, higher accuracy and enable higher learning rates. To disentangle how these benefits are related, we train a batch normalized network using the learning rate and the number of epochs of an unnormalized network, as well as an initial learning rate of $\alpha = 0.003$ which requires 1320 epochs for training. These results are also illustrated in Figure 1, where we see that a batch normalized networks with such a low learning schedule performs no better than an unnormalized network. Additionally, the train-test gap is much larger than for normalized networks using lr $\alpha = 0.1$, indicating more overfitting. A learning rate of $\alpha = 0.003$ gives results in between these extremes. This suggests that it is the higher learning rate that BN enables, which mediates the majority of its benefits; it improves regularization, accuracy and gives faster convergence. Similar results can be shown for variants of BN, see Table 4 in Appendix K of the online version [4].

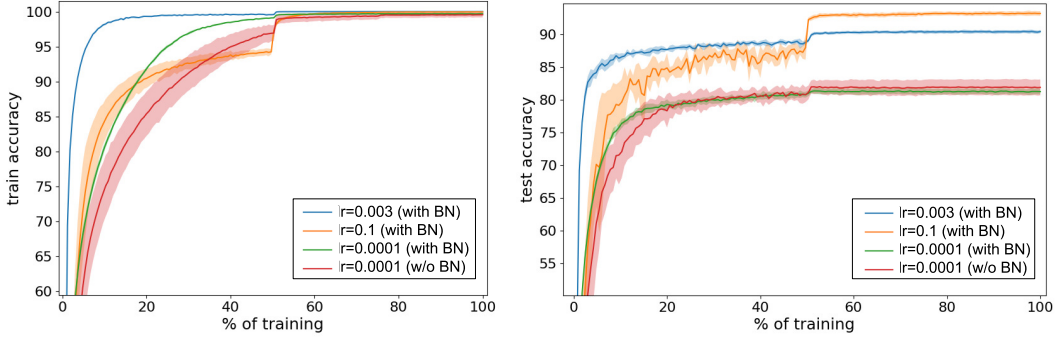


Figure 1: The training (*left*) and testing (*right*) accuracies as a function of progress through the training cycle. We used a 110-layer Resnet with three distinct learning rates 0.0001, 0.003, 0.1. The smallest, 0.0001 was picked such that the network without BN converges. The figure shows that with matching learning rates, both networks, with BN and without, result in comparable testing accuracies (red and green lines in right plot). In contrast, larger learning rates yield higher test accuracy for BN networks, and diverge for unnormalized networks (not shown). All results are averaged over five runs with std shown as shaded region around mean.

2.1 Learning rate and generalization

To explain these observations we consider a simple model of SGD; the loss function $\ell(x)$ is a sum over the losses of individual examples in our dataset $\ell(x) = \frac{1}{N} \sum_{i=1}^N \ell_i(x)$. We model SGD as sampling a set B of examples from the dataset with replacements, and then with learning rate α estimate the gradient step as $\alpha \nabla_{SGD}(x) = \frac{\alpha}{|B|} \sum_{i \in B} \nabla \ell_i(x)$. If we subtract and add $\alpha \nabla \ell(x)$ from this expression we can restate the estimated gradient $\nabla_{SGD}(x)$ as the true gradient, and a noise term

$$\alpha \nabla_{SGD}(x) = \underbrace{\alpha \nabla \ell(x)}_{\text{gradient}} + \underbrace{\frac{\alpha}{|B|} \sum_{i \in B} (\nabla \ell_i(x) - \nabla \ell(x))}_{\text{error term}}.$$

We note that since we sample uniformly we have $\mathbb{E} \left[\frac{\alpha}{|B|} \sum_{i \in B} (\nabla \ell_i(x) - \nabla \ell(x)) \right] = 0$. Thus the gradient estimate is unbiased, but will typically be noisy. Let us define an architecture dependent noise quantity C of a single gradient estimate such that $C = \mathbb{E} [\|\nabla \ell_i(x) - \nabla \ell(x)\|^2]$. Using basic linear algebra and probability theory, see Appendix D, we can upper-bound the noise of the gradient step estimate given by SGD as

$$\mathbb{E} [\|\alpha \nabla \ell(x) - \alpha \nabla_{SGD}(x)\|^2] \leq \frac{\alpha^2}{|B|} C. \quad (2)$$

Depending on the tightness of this bound, it suggests that the noise in an SGD step is affected similarly by the learning rate as by the inverse mini-batch size $\frac{1}{|B|}$. This has indeed been observed in practice in the context of parallelizing neural networks [14, 49] and derived in other theoretical models [24]. It is widely believed that the noise in SGD has an important role in regularizing neural networks [6, 57]. Most pertinent to us is the work of Keskar et al. [25], where it is empirically demonstrated that large mini-batches lead to convergence in sharp minima, which often generalize poorly. The intuition is that larger SGD noise from smaller mini-batches prevents the network from getting “trapped” in sharp minima and therefore bias it towards wider minima with better generalization. Our observation from (2) implies that SGD noise is similarly affected by the learning rate as by the inverse mini-batch size, suggesting that a higher learning rate would similarly bias the network towards wider minima. We thus argue that the better generalization accuracy of networks with BN, as shown in Figure 1, can be explained by the higher learning rates that BN enables.

3 Batch Normalization and Divergence

So far we have provided empirical evidence that the benefits of batch normalization are primarily caused by higher learning rates. We now investigate why BN facilitates training with higher learning rates in the first place. In our experiments, the maximum learning rates for unnormalized networks

have been limited by the tendency of neural networks to *diverge* for large rates, which typically happens in the first few mini-batches. We therefore focus on the gradients at initialization. When comparing the gradients between batch normalized and unnormalized networks one consistently finds that the gradients of comparable parameters are larger and distributed with heavier tails in unnormalized networks. Representative distributions for gradients within a convolutional kernel are illustrated in Figure 2.

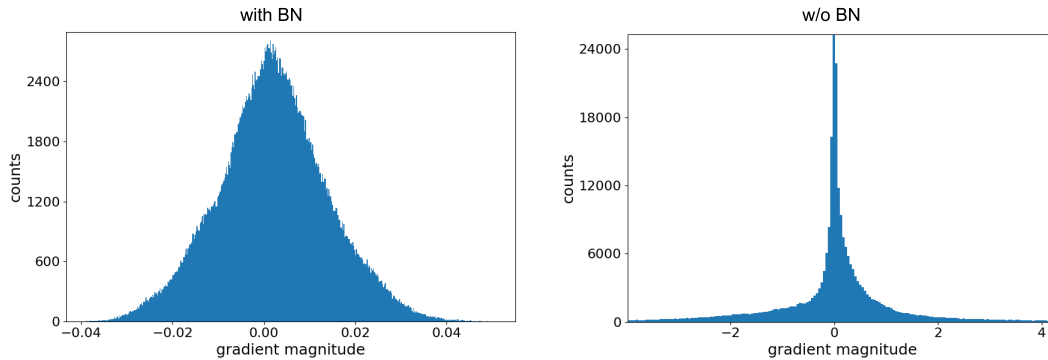


Figure 2: Histograms over the gradients at initialization for (midpoint) layer 55 of a network with BN (*left*) and without (*right*). For the unnormalized network, the gradients are distributed with heavy tails, whereas for the normalized networks the gradients are concentrated around the mean. (Note that we have to use different scales for the two plots because the gradients for the unnormalized network are almost two orders of magnitude larger than for the normalized on.)

A natural way of investigating divergence is to look at the loss landscape along the gradient direction during the first few mini-batches that occur with the normal learning rate (0.1 with BN, 0.0001 without). In Figure 3 we compare networks with and without BN in this regard. For each network we compute the gradient on individual batches and plot the relative change in loss as a function of the step-size (i.e. $\text{new_loss}/\text{old_loss}$). (Please note the different scales along the vertical axes.) For unnormalized networks only small gradient steps lead to reductions in loss, whereas networks with BN can use a far broader range of learning rates.

Let us define *network divergence* as the point when the loss of a mini-batch increases beyond 10^3 (a point from which networks have never managed to recover to acceptable accuracies in

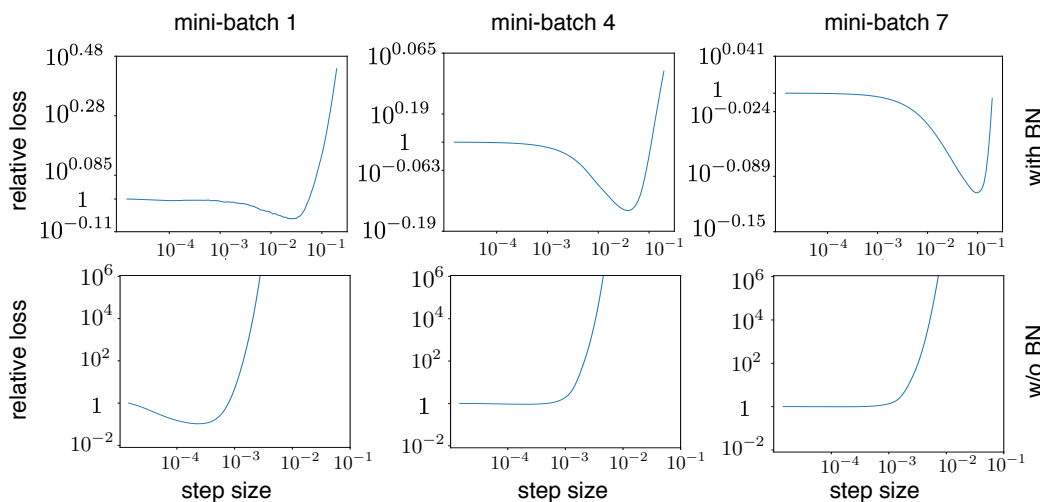


Figure 3: Illustrations of the relative loss over a mini-batch as a function of the step-size (normalized by the loss before the gradient step). Several representative batches and networks are shown, each one picked at the start of the standard training procedure. Throughout all cases the network with BN (bottom row) is far more forgiving and the loss decreases over larger ranges of α . Networks without BN show divergence for larger step sizes.

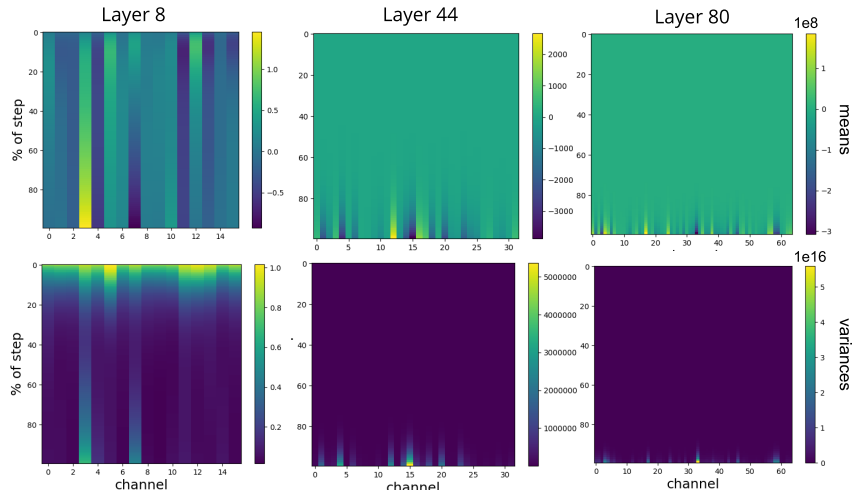


Figure 4: Heatmap of channel means and variances during a diverging gradient update (without BN). The vertical axis denote what percentage of the gradient update has been applied, 100% corresponds to the endpoint of the update. The moments explode in the higher layer (note the scale of the color bars).

our experiments). With this definition, we can precisely find the gradient update responsible for divergence. It is interesting to see what happens with the means and variances of the network activations along a 'diverging update'. Figure 4 shows the means and variances of channels in three layers (8,44,80) during such an update (without BN). The color bar reveals that the scale of the later layer's activations and variances is orders of magnitudes higher than the earlier layer. This seems to suggest that the divergence is caused by activations growing progressively larger with network depth, with the network output "exploding" which results in a diverging loss. BN successfully mitigates this phenomenon by correcting the activations of each channel and each layer to zero-mean and unit standard deviation, which ensures that large activations in lower levels cannot propagate uncontrollably upwards. We argue that this is the primary mechanism by which batch normalization enables higher learning rates – no matter how large of a gradient update is applied, the network will always "land safely" in a region without activations growing with network depth. Our explanation would suggest that the mean and variance μ, σ^2 used for normalization needs to be updated every batch for this "security guarantee" to hold, and in Table 3 in Appendix H we indeed verify that updating μ, σ^2 only every other batch does not enable high learning rates. This explanation is also consistent with the general folklore observations that shallower networks allow for larger learning rates, which we verify in Appendix H. In shallower networks there aren't as many layers in which the activation explosion can propagate.

4 Batch Normalization and Gradients

Figure 4 shows that the moments of unnormalized networks explode during network divergence and Figure 5 depicts the moments as a function of the layer depth after initialization (without BN) in log-scale. The means and variances of channels in the network tend to increase with the depth of the network even at initialization time — suggesting that a substantial part of this growth is data independent. In Figure 5 we also note that the network transforms normalized inputs into an output that reaches scales of up to 10^2 for the largest output channels. It is natural to suspect that such a dramatic relationship between output and input are responsible for the large gradients seen in Figure 2. To test this intuition, we train a Resnet that uses one batch normalization layer only at the very last layer of the network, normalizing the output of the last residual block but no intermediate activation. Such an architecture allows for learning rates up to 0.03 and yields a final test accuracy of 90.1%, see Appendix E — capturing two-thirds of the overall BN improvement (see Figure 1). This suggests that normalizing the final layer of a deep network may be one of the most important contributions of BN.

For the final output layer corresponding to the classification, a large channel mean implies that the network is biased towards the corresponding class. In Figure 6 we created a heatmap of $\frac{\partial L_b}{\partial O_{b,j}}$ after

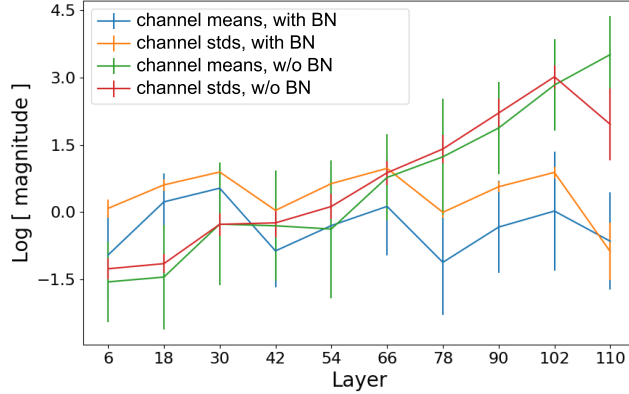


Figure 5: Average channel means and variances as a function of network depth at initialization (error bars show standard deviations) on log-scale for networks with and without BN. The batch normalized network the mean and variances stays relatively constant throughout the network. For an unnormalized network, they seem to grow almost exponentially with depth.

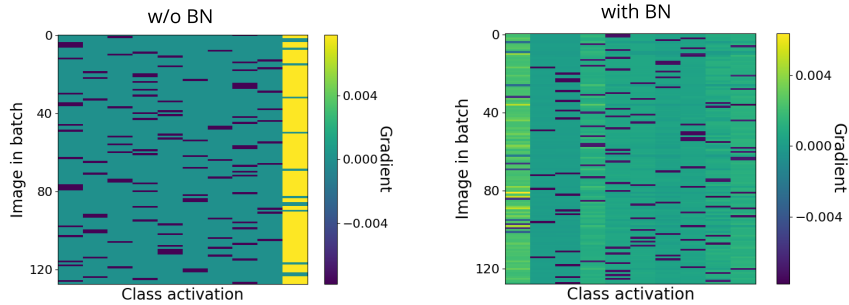


Figure 6: A heat map of the output gradients in the final classification layer after initialization. The columns correspond to a classes and the rows to images in the mini-batch. For an unnormalized network (*left*), it is evident that the network consistently predicts one specific class (very right column), irrespective of the input. As a result, the gradients are highly correlated. For a batch normalized network, the dependence upon the input is much larger.

initialization, where L_b is the loss for image b in our mini-batch, and activations j corresponds to class j at the final layer. A yellow entry indicates that the gradient is positive, and the step along the negative gradient would decrease the prediction strength of this class for this particular image. A dark blue entry indicates a negative gradient, indicating that this particular class prediction should be strengthened. Each row contains one dark blue entry, which corresponds to the true class of this particular image (as initially all predictions are arbitrary). A striking observation is the distinctly yellow column in the left heatmap (network without BN). This indicates that after initialization the network tends to almost always predict the same (typically wrong) class, which is then corrected with a strong gradient update. In contrast, the network with BN does not exhibit the same behavior, instead positive gradients are distributed throughout all classes. Figure 6 also sheds light onto why the gradients of networks without BN tend to be so large in the final layers: the rows of the heatmap (corresponding to different images in the mini-batch) are highly correlated. Especially the gradients in the last column are positive for almost all images (the only exceptions being those image that truly belong to this particular class label). The gradients, summed across all images in the minibatch, therefore consist of a sum of terms with matching signs and yield large absolute values. Further, these gradients differ little across inputs, suggesting that most of the optimization work is done to rectify a bad initial state rather than learning from the data.

4.1 Gradients of convolutional parameters

We observe that the gradients in the last layer can be dominated by some arbitrary bias towards a particular class. Can a similar reason explain why the gradients for convolutional weights are larger

	$a = \sum_{bxy} d_{c_o c_i i j}^{bxy} $	$b = \sum_{bij} d_{c_o c_i i j}^{bxy} $	a/b
Layer 18, with BN	7.5e-05	3.0e-07	251.8
Layer 54, with BN	1.9e-05	1.7e-07	112.8
Layer 90, with BN	6.6e-06	1.6e-07	40.7
Layer 18, w/o BN	6.3e-05	3.6e-05	1.7
Layer 54, w/o BN	2.2e-04	8.4e-05	2.6
Layer 90, w/o BN	2.6e-04	1.2e-04	2.1

Table 1: Gradients of a convolutional kernel as described in (4) at initialization. The table compares the absolute value of the sum of gradients, and the sum of absolute values. Without BN these two terms are similar in magnitude, suggesting that the summands have matching signs throughout and are largely data independent. For a batch normalized network, those two differ by about two orders of magnitude.

for unnormalized networks. Let us consider a convolutional weight $K_{o,i,x,y}$, where the first two dimensions correspond to the outgoing/ingoing channels and the two latter to the spatial dimensions. For notational clarity we consider 3-by-3 convolutions and define $S = \{-1, 0, 1\} \times \{-1, 0, 1\}$ which indexes into K along spatial dimensions. Using definitions from section 1.1 we have

$$O_{b,c,x,y} = \sum_{c'} \sum_{x',y' \in S} I_{b,c',x+x',y+y'} K_{c,c',x',y'} \quad (3)$$

Now for some parameter $K_{o,i,x,y}$ inside the convolutional weight K , its derivate with respect to the loss is given by the backprop equation [40] and (3) as

$$\frac{\partial L}{\partial K_{o,i,x',y'}} = \sum_{b,x,y} d_{o,i,x',y'}^{bxy}, \quad \text{where} \quad d_{o,i,x',y'}^{bxy} = \frac{\partial L}{\partial O_{b,o,x,y}} I_{b,i,x+x',y+y'}. \quad (4)$$

The gradient for $K_{o,i,x,y}$ is the sum over the gradients of examples within the mini-batch, and over the convoluted spatial dimensions. We investigate the signs of the summands in (4) across both network types and probe the sums at initialization in Table 1. For an unnormalized networks the absolute value of (4) and the sum of the absolute values of the summands generally agree to within a factor 2 or less. For a batch normalized network, these expressions differ by a factor of 10^2 , which explains the stark difference in gradient magnitude between normalized and unnormalized networks observed in Figure 2. These results suggest that for an unnormalized network, the summands in (4) are similar across both spatial dimensions and examples within a batch. They thus encode information that is neither input-dependent or dependent upon spatial dimensions, and we argue that the learning rate would be limited by the large input-independent gradient component and that it might be too small for the input-dependent component. We probe these questions further in Appendix J, where we investigate individual parameters instead of averages.

Table 1 suggests that for an unnormalized network the gradients are similar across spatial dimensions and images within a batch. It’s unclear however how they vary across the input/output channels i, o . To study this we consider the matrix $M_{i,o} = \sum_{xy} |\sum_{bxy} d_{oi xy}^{bxy}|$ at initialization, which intuitively measures the average gradient magnitude of kernel parameters between input channel i and output channel o . Representative results are illustrated in Figure 7. The heatmap shows a clear trend that some channels constantly are associated with larger gradients while others have extremely small gradients by comparison. Since some channels have large means, we expect in light of (4) that weights outgoing from such channels would have large gradients which would explain the structure in Figure 7. This is indeed the case, see Appendix G in the online version [4].

5 Random initialization

In this section argue that the gradient explosion in networks without BN is a natural consequence of random initialization. This idea seems to be at odds with the trusted Xavier initialization scheme [12] which we use. Doesn’t such initialization guarantee a network where information flows smoothly between layers? These initialization schemes are generally derived from the desiderata that the variance of channels should be constant when randomization is taken over random weights. We argue that this condition is too weak. For example, a pathological initialization that sets weights to 0 or

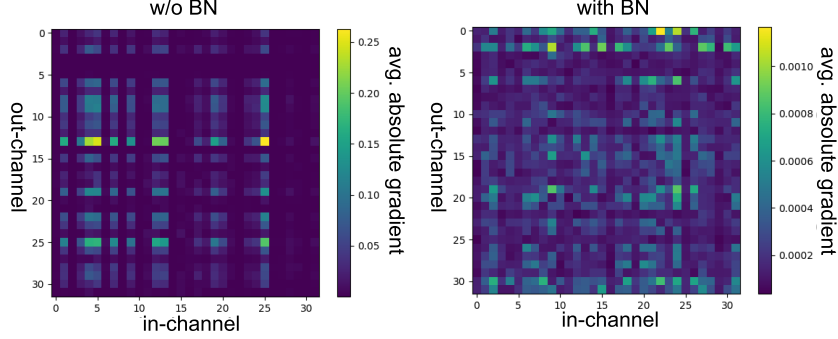


Figure 7: Average absolute gradients for parameters between in and out channels for layer 45 at initialization. For an unnormalized network, we observe a dominant low-rank structure. Some in/out-channels have consistently large gradients while others have consistently small gradients. This structure is less pronounced with batch normalization (*right*).

100 with some probability could fulfill it. In [12] the authors make simplifying assumptions that essentially result in a linear neural network. We consider a similar scenario and connect them with recent results in random matrix theory to gain further insights into network generalization. Let us consider a simple toy model: a linear feed-forward neural network where $A_t \dots A_2 A_1 x = y$, for weight matrices $A_1, A_2 \dots A_n$. While such a model clearly abstracts away many important points they have proven to be valuable models for theoretical studies [12, 15, 32, 56]. CNNs can, of course, be flattened into fully-connected layers with shared weights. Now, if the matrices are initialized randomly, the network can simply be described by a product of random matrices. Such products have recently garnered attention in the field of random matrix theory, from which we have the following recent result due to [30].

Theorem 1 *Singular value distribution of products of independent Gaussian matrices [30].* Assume that $X = X_1 X_2 \dots X_M$, where X_i are independent $N \times N$ Gaussian matrices s.t. $\mathbb{E}[X_{i,jk}] = 0$ and $\mathbb{E}[X_{i,jk}^2] = \sigma_i^2/N$ for all matrices i and indices j, k . In the limit $N \rightarrow \infty$, the expected singular value density $\rho_M(x)$ of X for $x \in (0, (M+1)^{M+1}/M^M)$ is given by

$$\rho_M(x) = \frac{1}{\pi x} \frac{\sin((M+1)\varphi)}{\sin(M\varphi)} \sin \varphi, \quad \text{where} \quad x = \frac{(\sin((M+1)\varphi))^{M+1}}{\sin \varphi (\sin(M\varphi))^M} \quad (5)$$

Figure 8 illustrates some density plots for various values of M and θ . A closer look at (5) reveals that the distribution blows up as $x^{-M/(M+1)}$ nears the origin, and that the largest singular value scales as $\mathcal{O}(M)$ for large matrices. In Figure 9 we investigate the singular value distribution for practically sized matrices. By multiplying more matrices, which represents a deeper linear network, the singular values distribution becomes significantly more heavy-tailed. Intuitively this means that the ratio between the largest and smallest singular value (the condition number) will increase with depth, which we verify in Figure 20 in Appendix K.

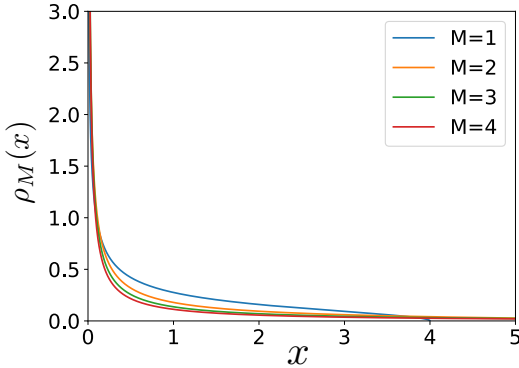


Figure 8: Distribution of singular values according to theorem 1 for some M . The theoretical distribution becomes increasingly heavy-tailed for more matrices, as does the empirical distributions of Figure 9

Consider $\min_{A_i, i=1,2 \dots t} \|A_t \dots A_2 A_1 x - y\|^2$, this problem is similar to solving a linear system $\min_x \|Ax - y\|^2$ if one only optimizes over a single weight matrix A_i . It is well known that the complexity of solving $\min_x \|Ax - y\|$ via gradient descent can be characterized by the condition number κ of A , the ratio between largest σ_{max} and smallest singular value σ_{min} . Increasing

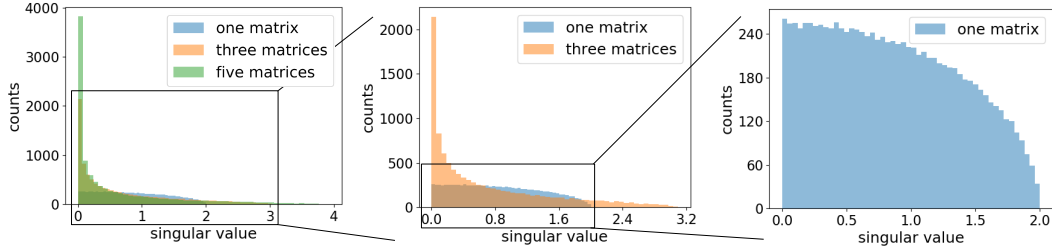


Figure 9: An illustration of the distributions of singular values of random square matrices and product of independent matrices. The matrices have dimension $N=1000$ and all entries independently drawn from a standard Gaussian distribution. Experiments are repeated ten times and we show the total number of singular values among all runs in every bin, distributions for individual experiments look similar. The left plot shows all three settings. We see that the distribution of singular values becomes more heavy-tailed as more matrices are multiplied together.

κ has the following effects on solving a linear system with gradient descent: **1)** convergence becomes slower, **2)** a smaller learning rate is needed, **3)** the ratio between gradients in different subspaces increases [3]. There are many parallels between these results from numerical optimization, and what is observed in practice in deep learning. Based upon Theorem 1, we expect the conditioning of a linear neural network at initialization for more shallow networks to be better which would allow a higher learning rate. And indeed, for an unnormalized Resnet one can use a much larger learning if it has only few layers, see Appendix H. An increased condition number also results in different subspaces of the linear regression problem being scaled differently, although the notion of subspaces are lacking in ANNs, Figure 5 and 7 show that the scale of channels differ dramatically in unnormalized networks. The Xavier [12] and Kaming initialization schemes [16] amounts to a random matrix with iid entries that are all scaled proportionally to $n^{-1/2}$, the same exponent as in Theorem 1, with different constant factors. Theorem 1 suggests that such an initialization will yield ill-conditioned matrices, independent of these scale factors. If we accept these shortcomings of Xavier-initialization, the importance of making networks robust to initialization schemes becomes more natural.

6 Related Work

The original batch normalization paper posits that internal covariate explains the benefits of BN [23]. We do not claim that internal covariate shift does not exist, but we believe that the success of BN can be explained without it. We argue that a good reason to doubt that the primary benefit of BN is eliminating internal covariate shift comes from results in [34], where an initialization scheme that ensures that all layers are normalized is proposed. In this setting, internal covariate shift would not disappear. However, the authors show that such initialization can be used instead of BN with a relatively small performance loss. Another line of work of relevance is [48] and [47], where the relationship between various network parameters, accuracy and convergence speed is investigated, the former article argues for the importance of batch normalization to facilitate a phenomenon dubbed 'super convergence'. Due to space limitations, we defer discussion regarding variants of batch normalization, random matrix theory, generalization as well as further related work to Appendix A in the online version [4].

7 Conclusions

We have investigated batch normalization and its benefits, showing how the latter are mainly mediated by larger learning rates. We argue that the larger learning rate increases the implicit regularization of SGD, which improves generalization. Our experiments show that large parameter updates to unnormalized networks can result in activations whose magnitudes grow dramatically with depth, which limits large learning rates. Additionally, we have demonstrated that unnormalized networks have large and ill-behaved outputs, and that this results in gradients that are input independent. Via recent results in random matrix theory, we have argued that the ill-conditioned activations are natural consequences of the random initialization.

Acknowledgements

We would like to thank Yexiang Xue, Guillaume Perez, Rich Bernstein, Zdzislaw Burda, Liam McAllister, Yang Yuan, Vilja Järvi, Marlene Berke and Damek Davis for help and inspiration. This research is supported by NSF Expedition CCF-1522054 and Awards FA9550-18-1-0136 and FA9550-17-1-0292 from AFOSR. KQW was supported in part by the III-1618134, III-1526012, IIS-1149882, IIS-1724282, and TRIPODS- 1740822 grants from the National Science Foundation, and generous support from the Bill and Melinda Gates Foundation, the Office of Naval Research, and SAP America Inc.

References

- [1] Martin Arjovsky, Amar Shah, and Yoshua Bengio. Unitary evolution recurrent neural networks. In *International Conference on Machine Learning*, pages 1120–1128, 2016.
- [2] Jimmy Lei Ba, Jamie Ryan Kiros, and Geoffrey E Hinton. Layer normalization. *arXiv preprint arXiv:1607.06450*, 2016.
- [3] Dimitri P Bertsekas and Athena Scientific. *Convex optimization algorithms*. Athena Scientific Belmont, 2015.
- [4] Johan Bjorck, Carla Gomes, and Bart Selman. Understanding batch normalization. *arXiv preprint arXiv:1806.02375*, 2018.
- [5] Pratik Chaudhari, Anna Choromanska, Stefano Soatto, and Yann LeCun. Entropy-sgd: Biasing gradient descent into wide valleys. *arXiv preprint arXiv:1611.01838*, 2016.
- [6] Pratik Chaudhari and Stefano Soatto. Stochastic gradient descent performs variational inference, converges to limit cycles for deep networks. *arXiv preprint arXiv:1710.11029*, 2017.
- [7] Yunpeng Chen, Jianan Li, Huaxin Xiao, Xiaojie Jin, Shuicheng Yan, and Jiashi Feng. Dual path networks. In *Advances in Neural Information Processing Systems*, pages 4470–4478, 2017.
- [8] Anna Choromanska, Mikael Henaff, Michael Mathieu, Gérard Ben Arous, and Yann LeCun. The loss surfaces of multilayer networks. In *Artificial Intelligence and Statistics*, pages 192–204, 2015.
- [9] Tim Cooijmans, Nicolas Ballas, César Laurent, Çağlar Gülçehre, and Aaron Courville. Recurrent batch normalization. *arXiv preprint arXiv:1603.09025*, 2016.
- [10] Chris de Sa. Advanced machine learning systems : lecture notes, 2017.
- [11] Alan Edelman. Eigenvalues and condition numbers of random matrices. *SIAM Journal on Matrix Analysis and Applications*, 9(4):543–560, 1988.
- [12] Xavier Glorot and Yoshua Bengio. Understanding the difficulty of training deep feedforward neural networks. In *Proceedings of the Thirteenth International Conference on Artificial Intelligence and Statistics*, pages 249–256, 2010.
- [13] Ian Goodfellow, Yoshua Bengio, and Aaron Courville. *Deep Learning*. MIT Press, 2016. <http://www.deeplearningbook.org>.
- [14] Priya Goyal, Piotr Dollár, Ross Girshick, Pieter Noordhuis, Lukasz Wesolowski, Aapo Kyrola, Andrew Tulloch, Yangqing Jia, and Kaiming He. Accurate, large minibatch sgd: training imagenet in 1 hour. *arXiv preprint arXiv:1706.02677*, 2017.
- [15] Moritz Hardt and Tengyu Ma. Identity matters in deep learning. *arXiv preprint arXiv:1611.04231*, 2016.
- [16] Kaiming He, Xiangyu Zhang, Shaoqing Ren, and Jian Sun. Delving deep into rectifiers: Surpassing human-level performance on imagenet classification. In *Proceedings of the IEEE international conference on computer vision*, pages 1026–1034, 2015.
- [17] Kaiming He, Xiangyu Zhang, Shaoqing Ren, and Jian Sun. Deep residual learning for image recognition. In *Proceedings of the IEEE conference on computer vision and pattern recognition*, pages 770–778, 2016.
- [18] Sepp Hochreiter. Untersuchungen zu dynamischen neuronalen netzen. *Diploma, Technische Universität München*, 91(1), 1991.
- [19] Sepp Hochreiter and Jürgen Schmidhuber. Flat minima. *Neural Computation*, 9(1):1–42, 1997.

- [20] Elad Hoffer, Itay Hubara, and Daniel Soudry. Train longer, generalize better: closing the generalization gap in large batch training of neural networks. In *Advances in Neural Information Processing Systems*, pages 1729–1739, 2017.
- [21] Gao Huang, Zhuang Liu, Kilian Q Weinberger, and Laurens van der Maaten. Densely connected convolutional networks. In *Proceedings of the IEEE conference on computer vision and pattern recognition*, volume 1, page 3, 2017.
- [22] Sergey Ioffe. Batch renormalization: Towards reducing minibatch dependence in batch-normalized models. In *Advances in Neural Information Processing Systems*, pages 1942–1950, 2017.
- [23] Sergey Ioffe and Christian Szegedy. Batch normalization: Accelerating deep network training by reducing internal covariate shift. In *International Conference on Machine Learning*, pages 448–456, 2015.
- [24] Stanislaw Jastrzebski, Zachary Kenton, Devansh Arpit, Nicolas Ballas, Asja Fischer, Yoshua Bengio, and Amos Storkey. Three factors influencing minima in sgd. *arXiv preprint arXiv:1711.04623*, 2017.
- [25] Nitish Shirish Keskar, Dheevatsa Mudigere, Jorge Nocedal, Mikhail Smelyanskiy, and Ping Tak Peter Tang. On large-batch training for deep learning: Generalization gap and sharp minima. *arXiv preprint arXiv:1609.04836*, 2016.
- [26] Günter Klambauer, Thomas Unterthiner, Andreas Mayr, and Sepp Hochreiter. Self-normalizing neural networks. In *Advances in Neural Information Processing Systems*, pages 972–981, 2017.
- [27] Alex Krizhevsky and Geoffrey Hinton. Learning multiple layers of features from tiny images. 2009.
- [28] César Laurent, Gabriel Pereyra, Philémon Brakel, Ying Zhang, and Yoshua Bengio. Batch normalized recurrent neural networks. In *Acoustics, Speech and Signal Processing (ICASSP), 2016 IEEE International Conference on*, pages 2657–2661. IEEE, 2016.
- [29] Yann LeCun, Léon Bottou, Genevieve B Orr, and Klaus-Robert Müller. Efficient backprop. In *Neural networks: Tricks of the trade*, pages 9–50. Springer, 1998.
- [30] Dang-Zheng Liu, Dong Wang, Lun Zhang, et al. Bulk and soft-edge universality for singular values of products of ginibre random matrices. In *Annales de l’Institut Henri Poincaré, Probabilités et Statistiques*, volume 52, pages 1734–1762. Institut Henri Poincaré, 2016.
- [31] Cosme Louart, Zhenyu Liao, and Romain Couillet. A random matrix approach to neural networks. *arXiv preprint arXiv:1702.05419*, 2017.
- [32] Haihao Lu and Kenji Kawaguchi. Depth creates no bad local minima. *arXiv preprint arXiv:1702.08580*, 2017.
- [33] Dominic Masters and Carlo Luschi. Revisiting small batch training for deep neural networks. *arXiv preprint arXiv:1804.07612*, 2018.
- [34] Dmytro Mishkin and Jiri Matas. All you need is a good init. *arXiv preprint arXiv:1511.06422*, 2015.
- [35] Carles Roger Riera Molina and Oriol Pujol Vila. Solving internal covariate shift in deep learning with linked neurons. *arXiv preprint arXiv:1712.02609*, 2017.
- [36] Behnam Neyshabur, Srinadh Bhojanapalli, David McAllester, and Nati Srebro. Exploring generalization in deep learning. In *Advances in Neural Information Processing Systems*, pages 5949–5958, 2017.
- [37] Jeffrey Pennington and Yasaman Bahri. Geometry of neural network loss surfaces via random matrix theory. In *International Conference on Machine Learning*, pages 2798–2806, 2017.
- [38] Jeffrey Pennington and Pratik Worah. Nonlinear random matrix theory for deep learning.
- [39] James Renegar. Incorporating condition measures into the complexity theory of linear programming. *SIAM Journal on Optimization*, 5(3):506–524, 1995.
- [40] David E Rumelhart, Geoffrey E Hinton, and Ronald J Williams. Learning representations by back-propagating errors. *nature*, 323(6088):533, 1986.
- [41] Sirpa Saariinen, Randall Bramley, and George Cybenko. Ill-conditioning in neural network training problems. *SIAM Journal on Scientific Computing*, 14(3):693–714, 1993.

- [42] Tim Salimans and Diederik P Kingma. Weight normalization: A simple reparameterization to accelerate training of deep neural networks. In *Advances in Neural Information Processing Systems*, pages 901–909, 2016.
- [43] Fabian Schilling. The effect of batch normalization on deep convolutional neural networks, 2016.
- [44] Samuel S Schoenholz, Justin Gilmer, Surya Ganguli, and Jascha Sohl-Dickstein. Deep information propagation. *arXiv preprint arXiv:1611.01232*, 2016.
- [45] Hidetoshi Shimodaira. Improving predictive inference under covariate shift by weighting the log-likelihood function. *Journal of statistical planning and inference*, 90(2):227–244, 2000.
- [46] David Silver, Julian Schrittwieser, Karen Simonyan, Ioannis Antonoglou, Aja Huang, Arthur Guez, Thomas Hubert, Lucas Baker, Matthew Lai, Adrian Bolton, et al. Mastering the game of go without human knowledge. *Nature*, 550(7676):354, 2017.
- [47] Leslie N Smith. A disciplined approach to neural network hyper-parameters: Part 1—learning rate, batch size, momentum, and weight decay. *arXiv preprint arXiv:1803.09820*, 2018.
- [48] Leslie N Smith and Nicholay Topin. Super-convergence: Very fast training of residual networks using large learning rates. *arXiv preprint arXiv:1708.07120*, 2017.
- [49] Samuel L Smith, Pieter-Jan Kindermans, and Quoc V Le. Don’t decay the learning rate, increase the batch size. *arXiv preprint arXiv:1711.00489*, 2017.
- [50] Samuel L Smith and Quoc V Le. A bayesian perspective on generalization and stochastic gradient descent. 2018.
- [51] D Ulyanov, A Vedaldi, and VS Lempitsky. Instance normalization: The missing ingredient for fast stylization. *corr (2016)*. *arXiv preprint arXiv:1607.08022*.
- [52] Patrick Van Der Smagt and Gerd Hirzinger. Solving the ill-conditioning in neural network learning. In *Neural networks: tricks of the trade*, pages 193–206. Springer, 1998.
- [53] Shuang Wu, Guoqi Li, Lei Deng, Liu Liu, Yuan Xie, and Luping Shi. L1-norm batch normalization for efficient training of deep neural networks. *arXiv preprint arXiv:1802.09769*, 2018.
- [54] Yuxin Wu and Kaiming He. Group normalization. *arXiv preprint arXiv:1803.08494*, 2018.
- [55] Lechao Xiao, Yasaman Bahri, Jascha Sohl-Dickstein, Samuel S Schoenholz, and Jeffrey Pennington. Dynamical isometry and a mean field theory of cnns: How to train 10,000-layer vanilla convolutional neural networks. *arXiv preprint arXiv:1806.05393*, 2018.
- [56] Chulhee Yun, Suvrit Sra, and Ali Jadbabaie. Global optimality conditions for deep neural networks. *arXiv preprint arXiv:1707.02444*, 2017.
- [57] Chiyuan Zhang, Samy Bengio, Moritz Hardt, Benjamin Recht, and Oriol Vinyals. Understanding deep learning requires rethinking generalization. *arXiv preprint arXiv:1611.03530*, 2016.
- [58] Tullio Zolezzi. Condition number theorems in optimization. *SIAM Journal on Optimization*, 14(2):507–516, 2003.

Appendices

A Extended related work

A.1 On internal covariate shift and other explanations

The benefits of normalizing the inputs when training neural networks was known already in the 90s [29], here the rationale was that nonzero means biased the gradient updates. In the original BN paper [23], *internal covariate shift*, a concept dating back to [45], is proposed as the problem that BN alleviates. Internal covariate shift is explained as the tendency for features that some intermediate layer trains against to shift during training, although no precise formal definition is given. This explanation seems to have been deemed satisfying in some papers [53] [35], while other papers credits the succes of normalization to improved conditioning [42] or stability of concurrent updates [13]. The only work on empirically on batch normalization known to us is the master thesis [43], where most benefits of batch normalization are verified and where the interaction with batch normalization and activation functions are studied. This paper instead takes an first-principles approach to understanding batch normalization, we do not claim that internal covariate shift does not exist, but we believe that the success of BN can be explained without it. Indeed, as internal covariate shift is only vaguely defined, falsifying becomes hard.

A.2 Random matrix theory and conditioning

The classical definition of conditioning for linear systems is well known [3], but for general optimization problems there are other metric for conditioning [58] [39]. In the 90s there was some work on the conditioning of training sigmoid neural networks, see for example [52] [41], where the main focus seems to have been the conditioning of the Hessian matrix and ways to improve it. For modern neural networks conditioning is sometimes mentioned in passing, see for example [42], but there is little work focusing specifically defining and empirically studying conditioning. Random matrix theory has previously been used for broadly studying neural networks, see for example [38] [37] [31] [8]. Unlike this work, we consider products of random matrices, for which theory has recently been developed. The conditioning of random matrices in the context of solving a linear system has been studied by [11], where the conditioning and running time of conjugate gradient descent is studied as functions of the matrix size. Conditioning is also implicit in works on initialization of neural networks, where one naturally wants to facilitate ease of optimization and avoid exploding/vanishing gradients [18]. For example, [55] have recently proposed methods that allows for training of extremely deep networks without batch normalization, by using a more sophisticated analysis than [12]. Similarly, [44] uses mean-field theory to develop limits for information propagation, arguing for the importance of initializing close to order-to-chaos phase transitions. In the context of RNNs, [1] have proposed methods that avoid exploding/vanishing gradients by using structured matrices as building blocks for unitary layers.

A.3 Alternatives to Batch Normalization

Many alternatives to batch normalization have been proposed [42] [26] [22], however, the original formulation remains the most popular and is generally competitive with alternatives for image classification. For recurrent neural networks it is problematic to apply batch normalization [28] and to rectify this normalization schemes for RNNs have been proposed [9] [2]. In the distributed setting where a single batch is split among workers communicating batch statistics comes with communication overhead, to alleviate this [20] has proposed to let workers calculate their statistics independently, the paper additionally derives similar results as us for the relationship between batch size and learning rates. Some of these papers above have mentioned that normalization techniques improve conditioning [42], while others have mentioned the stability of concurrent updates [13]. However, these issues are typically mentioned in passing and mathematical rationale are rarely given.

A.4 Generalization in deep learning

Our work corroborates the emerging consensus regarding the approximate equivalence between batch size and learning rates [49] [14] [24] [33], the importance of the regularizing effects of SGD and

it’s relationship to generalization [25] [57] [6]. While [25] argues for the importance of small batch sizes, [50] gives a more nuanced picture, claiming that there is an optimal batch size and that [25] have focused on sizes above this optimal size. Other relevant work regarding generalization within deep learning are [19] [5] [36]. Of interest is also the work of [47], where the relationship between network parameters are explored further.

B Details on experimental setup

Our setup follows that of the original RESNET paper [17] – we consider image classification on CIFAR10 [27]. We use the original RESNET architecture for CIFAR10 with depth 110 as described in [17]. As per [17] we train our model with the cross-entropy using SGD with momentum (0.9) and weight decay ($5e-4$), using a batch size 128. We use standard image preprocessing of channel-wise mean and variance normalization and standard data augmentation of random horizontal flipping and random 32-by-32 cropping with 4-pixel zero-padding. For initialization, we use the Xavier-scheme [12]. Code can be obtained upon request to the first author.

When batch normalization is removed, the learning rates and the number of iterations need to be changed for satisfying performance. We standardize the learning rate and number of epochs used in our experiments as follows. We consider the initial learning rates from the set $\{0.1, 0.003, 0.001, 0.0003, 0.0001, 0.00003\}$ and report the best result, as measured by test accuracy at termination, for every architecture. Initially, all models are trained for 165 epochs and as in [17] we divide the learning rate by 10 after epoch 50% and 75%, at which point learning has typically plateaued. If learning doesn’t plateau for some number of epochs, we roughly double the number of epochs until it does.

Our code is implemented in pytorch and has been run on AWS p3.2xlarge instances. The source code for all experiments is to be made publically available at a later date. We chose the CIFAR10 dataset for its low computational overhead, and since its size allows us to manually analyze all components of the architecture and dataset. RESNET, on the other hand, is a widely familiar architecture that achieves results close to the state of the art, additionally, it is the basis for later architectural development [21] [7].

C Distribution of the singular values

The distribution for singular values of products of matrices have been found the limit of large matrices, we will follow the exposition of [30]. For the product of M matrices random matrices, the density $\rho(x)$ is most easily expressed in terms of φ , which is related to x as follows

$$x = \frac{(\sin((M + 1)\varphi))^{M+1}}{\sin \varphi (\sin(M\varphi))^M}, \quad 0 < \varphi < \frac{\pi}{M + 1} \tag{6}$$

We plot this relationship in Figure 10. Noting that this parametrization is strictly decreasing in φ it clearly gives a one-to-one mapping between x and φ . Given this parametrization, the density is given as follows

$$\rho(\varphi) = \frac{1}{\pi x} \frac{\sin((M + 1)\varphi)}{\sin(M\varphi)} \sin \varphi \tag{7}$$

The expression is complicated, however we can note that it blows up as $x \rightarrow 0$. In Figure 10 show the relationship between x and φ defined by (6). In Figure 8 in the main text we plot the expression (7) for some values of M .

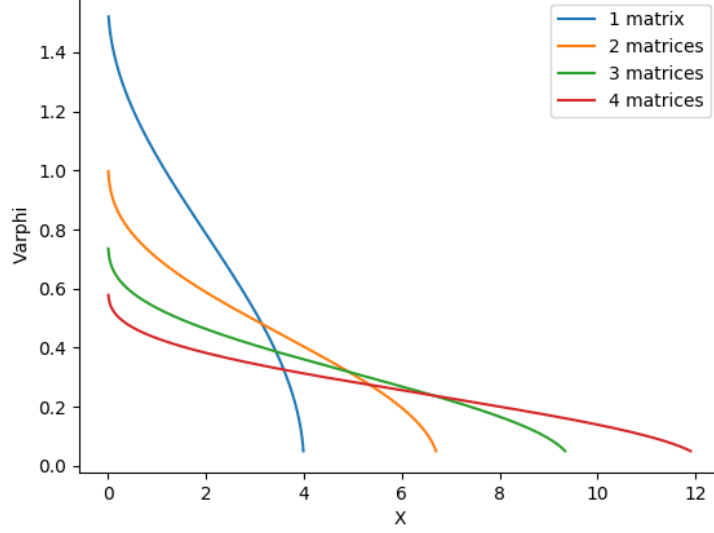


Figure 10: We here plot the relationship between x and φ according to (6) for different number of matrices multiplied together. We note that the relationship is injective.

D Deriving variance of SGD update

The relationship between learning rate and batch size has been observed elsewhere [24], our derivation is similar to [10]. Recall our loss function $\ell(x) = \sum_{i=1}^N \ell_i(x)$, when using a minibatch B we want to bound

$$\mathbb{E} \left[\left\| \frac{1}{|B|} \sum_{i \in B} \nabla \ell_i(x) - \nabla \ell(x) \right\|^2 \right] \quad (8)$$

Let us define $\Delta_i = \nabla \ell_i(x) - \nabla \ell(x)$ and take γ_i to be an indicator variable equal to one if example i is in batch B and zero else. We then have

$$(8) = \frac{1}{|B|} \mathbb{E} \left[\sum_{i=1}^N \sum_{j=1}^N \gamma_i \gamma_j \Delta_i^T \Delta_j \right]$$

Let us define $b = |B|$. Now, since samples are drawn independently we have $\mathbb{E}[\gamma_i \gamma_i] = \frac{b}{N}$ and $\mathbb{E}[\gamma_i \gamma_j] = \frac{b^2}{N^2}$. Thus we have

$$\begin{aligned} (8) &= \mathbb{E} \left[\frac{b^2}{N^2} \sum_{i \neq j} \Delta_i^T \Delta_j + \frac{b}{N} \sum_{i=1}^N \|\Delta_i\|^2 \right] \\ &= \frac{1}{bN} \mathbb{E} \left[\frac{b}{N} \sum_{i,j} \Delta_i \Delta_j + \left(1 - \frac{b}{N}\right) \sum_{i=1}^N \|\Delta_i\|^2 \right] \end{aligned}$$

Now, since the gradient estimate is unbiased, the first term vanishes. Under our assumption $\mathbb{E}[\|\nabla \ell_i(x) - \nabla \ell(x)\|^2] \leq C$ we now have

$$(8) = \frac{N-b}{bN^2} \mathbb{E} \left[\sum_{i=1}^N \|\Delta_i\|^2 \right] = \frac{N-b}{bN} \mathbb{E} \left[\frac{1}{N} \sum_{i=1}^N \|\nabla f_i(x) - \nabla f(x)\|^2 \right] \leq \frac{C}{b}$$

E BN on top

In Figure 11 and 12 we show the learning curves for a network that uses batch normalization only at the top of the network, right after the output of the residual blocks and right before the average pooling leading into the fully connected layer. With such an architecture, one gets only somewhat weaker performance than a completely batch normalized network, using a learning rate of 0.03 and 330 epochs.

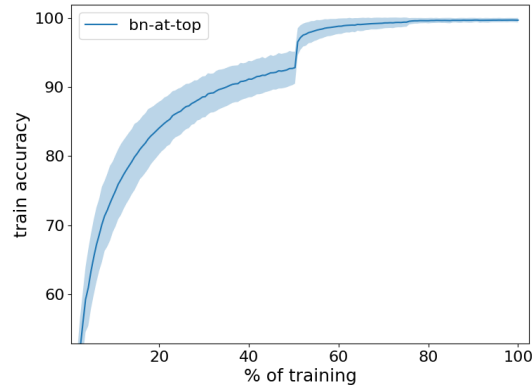


Figure 11: We here illustrate the training accuracy for an architecture where batch normalization is used only at the network top.

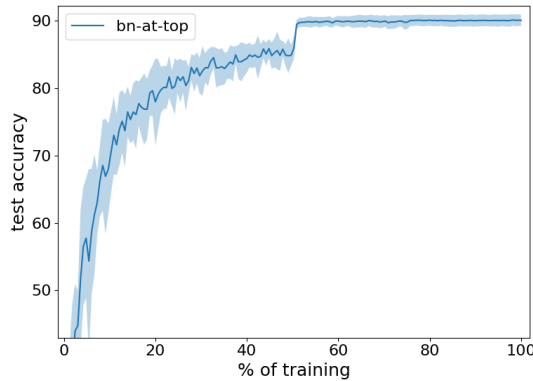


Figure 12: We here illustrate the test accuracy for an architecture where batch normalization is used only at the network top.

F The parts of batch normalization

Having seen the dramatic benefits of batch normalization, we now turn our attention to investigate the impact of the normalization and the affine transformation in (1) individually. We investigate the impact of the affine transformation by simply removing the parameters γ, β and the transformations they encode from the batch normalization algorithm, and then training the network. Results are illustrated to the left in Figure 13. The whole affine transformation improves the final accuracy only by roughly 0.6%, and while far from inconsequential the affine transformation introduces additional parameters which typically improves accuracy. The effect of the normalization in (1) is similarly investigated by removing those components, results in the absence of any affine transformation are shown to the right in Figure 13. When normalization is turned off, smaller learning rates and longer training is necessary however we consistently find that the highest learning rates that don't diverge give the best results, see Table 2. We see that the normalization has much more dramatic effects on accuracy and enables larger learning rate and faster convergence, but that both the mean and variance normalization are important.

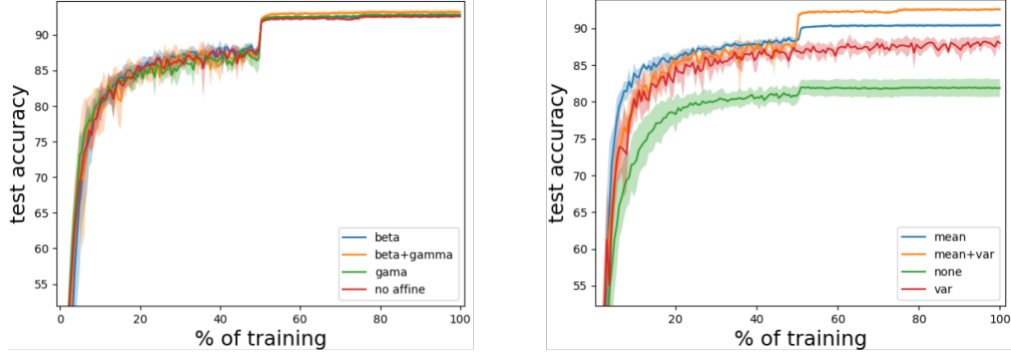


Figure 13: Illustrated above is the training curve for a 110-layer Resnet where parts of the batch norm algorithm are disabled. All experiments are repeated five times, with the shaded region corresponding to standard deviation and the thick lines the mean. To the left we illustrate the effect of the affine transformation parametrized by γ and β in (1), when mean and variance normalization is used. To the right, we illustrate the effect of the mean and variance normalization in absence of the affine transformation. The mean and standard deviation over five runs are indicated by thick and opaque lines respectively.

Architecture	Initial learning rate	Epochs
$\gamma, \beta, \mu, \sigma^2$	0.1	165
γ, μ, σ^2	0.1	165
β, μ, σ^2	0.1	165
μ, σ^2	0.1	165
σ^2	0.01	330
μ	0.003	330
None	0.0001	2640

Table 2: The optimal learning parameters when different components of batch normalization are used. The architecture represents the components that are used in (1)

G Explaining Figure 7

G.1 The effect of non-zero means

In Figure 5 we note that the means of different channels are nonzero in general. In histograms of the activations for an unnormalized network, one sees that some channels are essentially always on or always off, as their activations before Relu almost always have the same sign, see Figures 22 and 23 in Appendix K. Let us consider how this affects the gradients. If we calculate the loss L on one example and take neurons i, j with activations z_i, z_j to be connected between adjacent layers by weight w_{ij} within a feed-forward network, the gradients are given by backpropagation equation [40] as

$$\frac{\partial L}{\partial w_{ij}} = z_i \frac{\partial L}{\partial z_j} \quad (9)$$

We see in (9) that the derivative of w_{ij} scales linearly with the activation z_i . Thus, if some channel has a large mean we expect the gradient of weights outgoing from these channels to be large. To investigate this we plot the average gradient calculated over the dataset versus the mean channel activations for all kernel parameters. The results for layer 35 are illustrated in Figure 14 and as we can see the channel means have a large impact on the gradients. We also see that batch normalization essentially removes this dependence, so that the gradients of all channels have essentially the same scale.

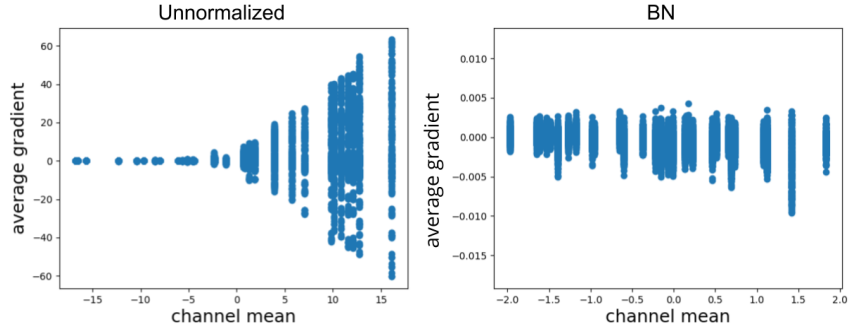


Figure 14: Here we illustrate the relationship between channel mean and gradients. Each point represents a single weight in a convolutional kernel, the x-axis is the mean activation before Relu for the in-channel of that weight while the y-axis is the average gradient of that weight at initialization. For an unnormalized network, large negative means leads to some channels being 'dead' after Relu such that their gradients are extremely small, while channels with large positive means have larger gradients. When using batch normalization this relationship disappears and all channels have equally large gradients on average.

G.2 Channel gradients

Let us again consider the backpropagation equation (9) for a feed-forward network, where we calculate the loss L on one example and take neurons i, j with activations z_i, z_j to be connected between adjacent layers by weight w_{ij} . In the linear model, we can view the neuron j is the input to the linear neural network ahead, which is simply a matrix. If a SVD-subspace that j is the input to has a large singular value it has a large impact on the output, and we expect the gradient $\frac{\partial L}{\partial z_j}$ to be large, which in turn makes $\frac{\partial L}{\partial w_{ij}}$ large. Within a single layer, the gradients will be scaled differently according to which subspaces they belong to, and with higher condition number κ the difference between these scales would increase. We investigate whether this intuition holds in our non-linear convolutional networks. In Figure 15 we plot gradients of the convolutional channels which are equivalent to the gradients of the bias terms. We see that the magnitude of the gradients differs a lot in earlier layers while being similarly scaled in higher layers. This is expected since the depth of the network "ahead" of lower layers are deeper for the early layers, which would cause them to have worse conditioning according to previous observations in RMT.

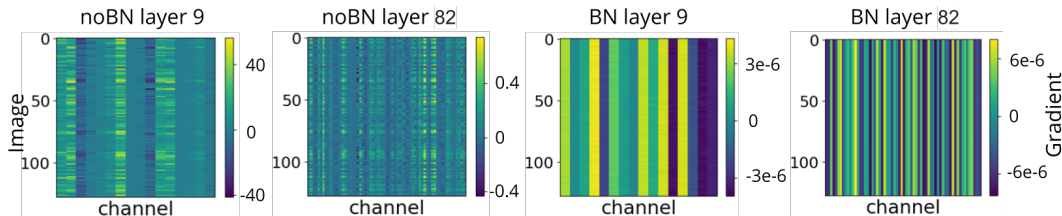


Figure 15: We here plot the gradients of the convolutional channels for the unnormalize and batch normalized network. We see that the gradients have larger scales for early layers in the unnormalized network, but not in later layers. With batch normalization, the gradients are similarly scaled across all layers.

H Learning rates for other architectures

We here give the highest initial learning rates achievable for some miscellaneous architectures, considering learning rates in the set $\{0.1, 0.003, 0.001, 0.0003, 0.0001, 0.00003\}$. We consider the original Resnet architecture with 32 and 56 layers respectively, and also an unnormalized network where we first train for one epoch with learning rate 0.0001. We refer to this as a warm start. This strategy allows us to study the ability of the network to rectify artifacts from the initialization. We also consider the scheme where the mean and variances are computed every other batch, and for other batches the latest moments are used. This strategy is referred to as Alternating normalization. Achievable learning rates are rates for which the networks don't diverge or remain at the accuracy

of random guessing. The results are illustrated in Table 3. We have additionally investigated the maximal learning rate that a batch normalized network can tolerate without diverging, and found the network to not diverge for 3.0 but diverge for 10.0.

Architecture	Initial learning rate
32 layer Resnet	0.1
56 layer Resnet	0.01
Unnormalized, warm start	0.01
Alternating normalization	0.01

Table 3: We here give the highest achievable learning rates for which some miscellaneous architectures. We see that less deep Resnets enables larger learning rates, and that warm-starting unnormalized nets allow for higher learning rates.

I Class-wise experiments

We here investigate how the different channels at the top layer, corresponding to the different unique classes we wish to classify, influence the gradients. In Figure 5 we have seen that the channel means increase with network depth, and in Figure 6 we have seen that this causes the network to always guess one specific class c at initialization. This, in turn, biases the gradients w.r.t. the activations at the top layer corresponding to class c to be larger. One would suspect that the gradients of all network parameters are primarily computed by their influence over the activations corresponding to class c . To investigate this we simply do a class-wise mask of the gradients that are being propagated from the top layer. We set $\frac{\partial L}{\partial z_{ij}}$, where z_{ij} is the activation for example i within a mini-batch and class j , to zero for all classes j except for one class j' and then backpropagate this information downwards in the network. This allows us to investigate the gradients of all network parameters w.r.t individual classes. In Figure 16 we show that indeed one class is responsible for the majority of the gradients for a representative convolutional kernel. This channel is the one class c that the network almost always guesses. We further investigate this in Figure 17 where we show that the dominant class c gives gradients that are at least one order of magnitude larger than other classes.

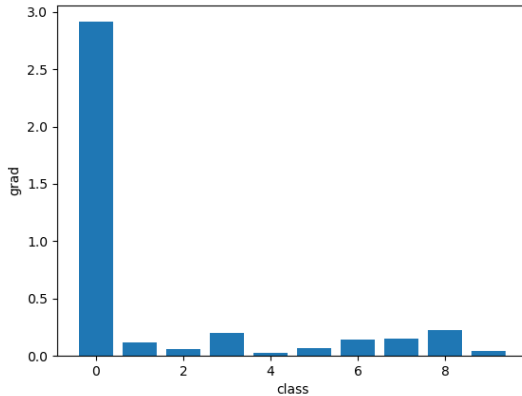


Figure 16: We here show how the absolute value of gradients for all parameters in the convolutional kernel in layer 52 are computed across the different classes at the top layer. It is clear that one specific class has far larger impact upon the gradients. Similar results are found for other layers.

J Kernel gradients experiments

According to (4) the gradients for one parameter in a convolutional kernel is given by $\sum_{b,x,y} d_{c_o c_i i j}^{bxy}$. In Table 1 we have seen that we have for an unnormalized network $|\sum_{b,x,y} d_{c_o c_i i j}^{bxy}| \approx \sum_{b,x,y} |d_{c_o c_i i j}^{bxy}|$ while these two differ by about two orders of magnitude at initialization. In Figure 18 we show

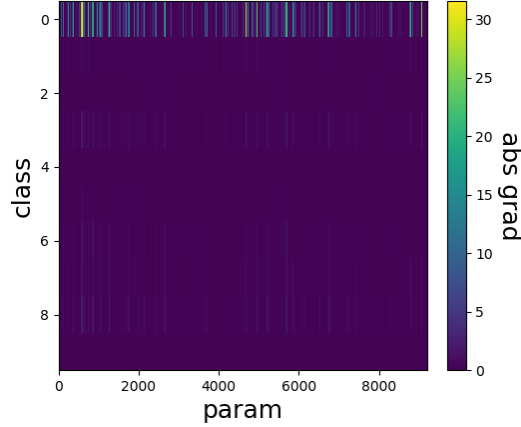


Figure 17: We here show the average absolute value of gradients for all parameters in the convolutional kernel in layer 52 across the different classes at the top layer. We see that one class has about one order of magnitude larger gradients than the other classes. Similar results are found for other layers.

how the terms $d_{c_o c_i i j}^{bxy}$ are distributed by a typical kernel parameter in an unnormalized network for which $|\sum_{b,x,y} d_{c_o c_i i j}^{bxy}| \approx \sum_{b,x,y} |d_{c_o c_i i j}^{bxy}|$ at initialization. Table 1 also just give summary statistics, to further investigate the relationship between $|\sum_{b,x,y} d_{c_o c_i i j}^{bxy}|$ and $\sum_{b,x,y} |d_{c_o c_i i j}^{bxy}|$ for individual parameters we plot a scatterplot of these two values for all parameters within a convolutional kernel. A typical result for both unnormalized and batch-normalized networks are shown in Figure 19.

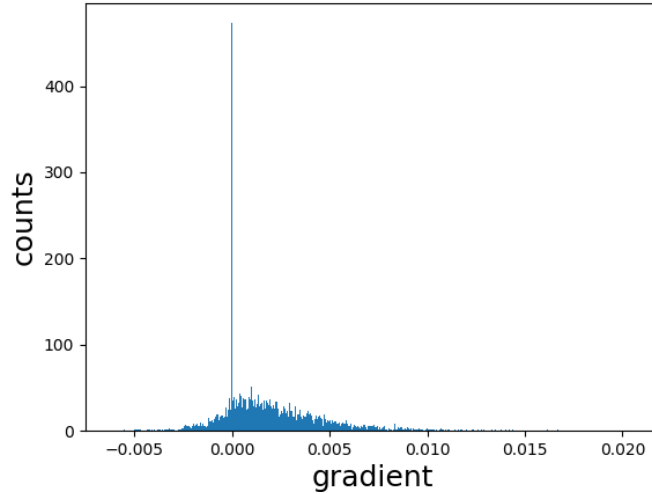


Figure 18: We here show the distribution of $d_{c_o c_i i j}^{bxy}$, defined as per (4), for a single parameter in layer 90 for which $|\sum_{b,x,y} d_{c_o c_i i j}^{bxy}| \approx \sum_{b,x,y} |d_{c_o c_i i j}^{bxy}|$. We see that not all gradients are identical, but that the distribution are skewed far from 0. For parameters with smaller gradients these distributions are typically centered around 0.

K Miscellaneous Experiments

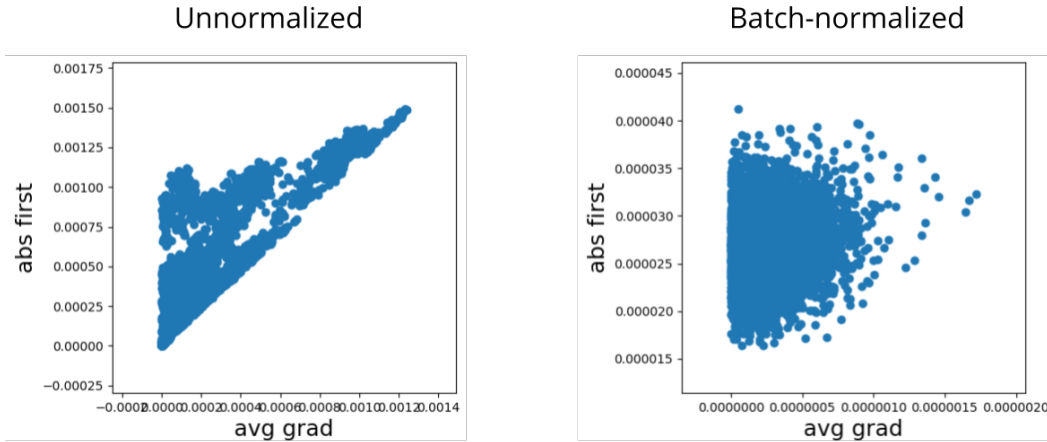


Figure 19: We here use the two values $|\sum_{b,x,y} d_{c_o c_i^{xy}}^{bxy}|$ and $\sum_{b,x,y} |d_{c_o c_i^{xy}}^{bxy}|$ for individual parameters in layer 54 as coordinates in a scatterplot. For an unnormalized networks we see an almost straight line that many parameters fall on, this represents parameters for which the gradients of the outgoing activations are similar across spatial dimensions and examples within a batch. For a normalized network this relationship disappears, and the gradients becomes much smaller.

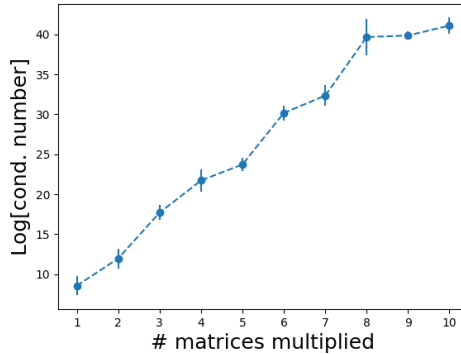


Figure 20: Above we illustrate the condition number κ of products of independent random square matrices as a function of the number of product matrices, the means and standard deviations over five runs are indicated with error bars. All matrices have size 1000 and entries independent gaussian entries, as we see, the condition number increases dramatically as the number of matrix products grows. Notice the logarithmic scale.

lr	0.1	0.01	0.003	0.0001
Groupnorm [54]	93.12	91.21	90.53	84.51
Instancenorm [51]	92.77	90.15	88.47	81.38
Layernorm [2]	85.40	91.68	89.46	85.10

Table 4: We here compare the results of training various normalization schemes with varying learning rates. Some of these schemes require slightly more training than BN to reach final performance. For lr 0.1 and 0.01 we use 660 epochs, for 0.003 we use 1320 epochs and for 0.0001 we use 2400 epochs. Generally the performance degrade with smaller learning rates for all techniques. Note, however, that layernorm seem to require a slightly smaller learning rate for optimal performance and we expect even smaller learning rate to further degrade its performance.

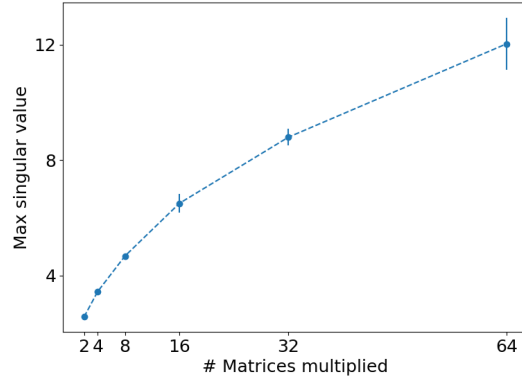


Figure 21: Above we illustrate the maximum singular value number of products of independent random square matrices as a function of the number of product matrices, the means and standard deviations over five runs are indicated with error bars. All matrices have size 1000 and entries independent gaussian entries, as we see, the maximum singular value increases as the number of matrix products grows, although not at the linear rate we would expect from infinitely large matrices.

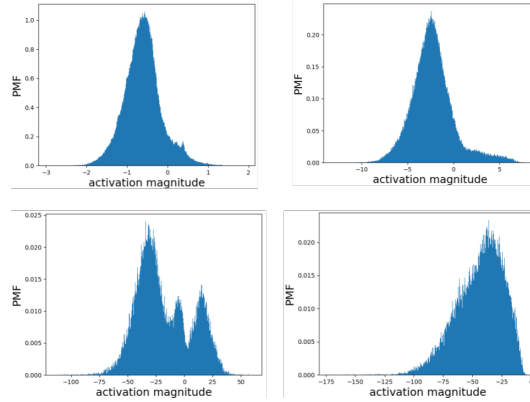


Figure 22: Above we illustrate some representative histograms over the activations for channels in different layers for an unnormalized network, sampled over spatial dimensions. Starting in the top left corner and going clockwise, the layers are 9, 45, 81 and 83. We see that for the deeper layers, the distributions increasingly have nonzero means and becomes more multimodal.

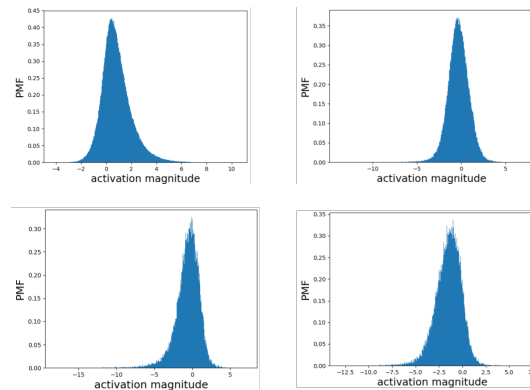


Figure 23: Above we illustrate some representative histograms over the activations for channels in different layers for a normalized network, sampled over spatial dimensions. Starting in the top left corner and going clockwise, the layers are 9, 45, 81 and 83. We see that the distributions remain unimodal with means close to zero, even deep into the network.

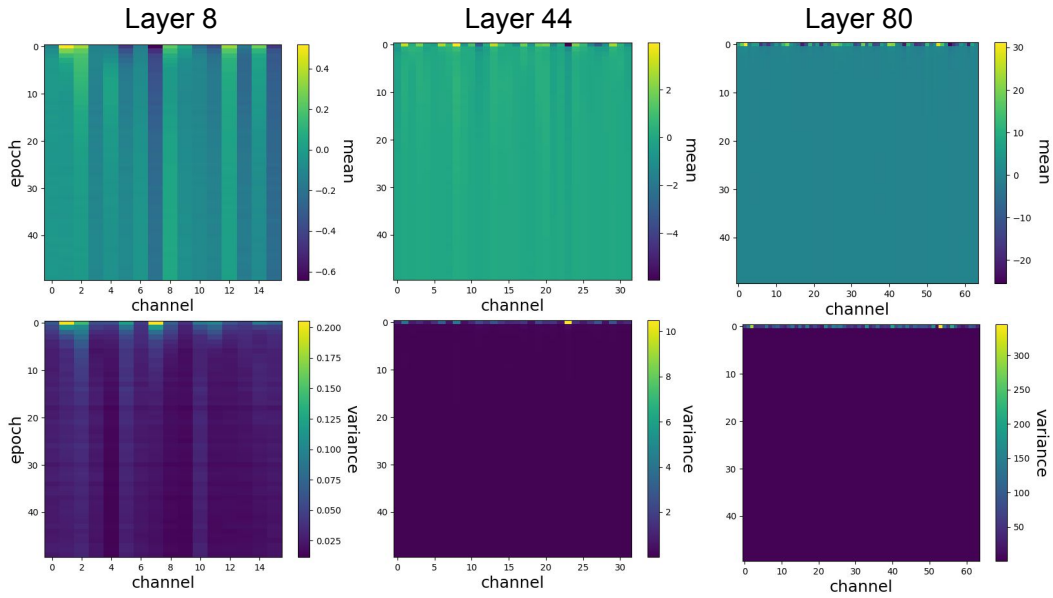


Figure 24: We here show how the moments of an unnormalized network, trained with learning rate 0.0001, changes during the first few batches of the first epoch. Illustrated here are the moments of individual channels, as they would be measured by batch normalization. Clearly, the activations becomes smaller and especially in the higher layers of the network both the mean and variance shrinks, suggesting that the gradients points towards smaller activations.

	$\sum_{bxy} d_{c_o c_i ij}^{bxy} $	$\sum_b \sum_{xy} d_{c_o c_i ij}^{bxy} $	$\sum_{xy} \sum_b d_{c_o c_i ij}^{bxy} $	$ \sum_{bij} d_{c_o c_i ij}^{bxy} $
Layer 18, BN	7.44509e-05	4.56393e-06	1.30080e-05	2.95631e-07
Layer 19, BN	5.20086e-05	3.42920e-06	9.15506e-06	2.62803e-07
Layer 54, BN	1.90210e-05	2.49563e-06	3.31031e-06	1.68555e-07
Layer 55, BN	1.62719e-05	2.16015e-06	2.82755e-06	1.70799e-07
Layer 90, BN	6.62426e-06	3.24293e-06	1.12625e-06	1.62689e-07
Layer 91, BN	5.44784e-06	3.07908e-06	9.09220e-07	1.98679e-07
Layer 18	6.31433e-05	3.65324e-05	4.06954e-05	3.63081e-05
Layer 19	5.34921e-05	1.99664e-05	2.90620e-05	1.95912e-05
Layer 54	2.19251e-04	8.63927e-05	1.54601e-04	8.35946e-05
Layer 55	6.82446e-05	2.08266e-05	4.50409e-05	1.95185e-05
Layer 90	2.59182e-04	1.59253e-04	1.80002e-04	1.23079e-04
Layer 91	1.37431e-04	8.61152e-05	9.31557e-05	6.46625e-05

Table 5: We here show the extended version of Table 1. In the Resnet architecture two consecutive layers play different roles, and thus we give values for neighboring layers.

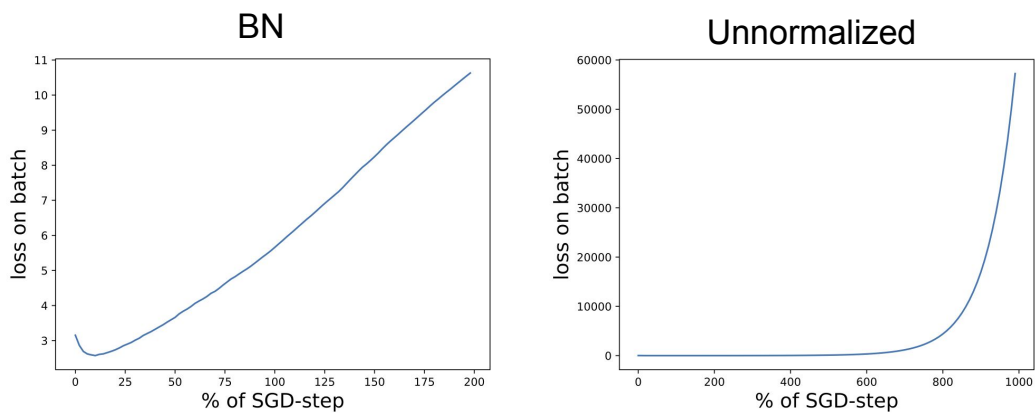


Figure 25: We here illustrate the loss along the gradient direction for a normalized and an unnormalized network, for the very first minibatch. Both of them show divergent behaviour during this first batch, but as seen in Figure 3 this behaviour is transient. For the unnormalized network the loss increases seemingly exponentially while it only increases linearly for the normalized network.